Bioorganic & Medicinal Chemistry 20 (2012) 6739–6750

Contents lists available at SciVerse ScienceDirect

Bioorganic & Medicinal Chemistry

journal homepage: www.elsevier.com/locate/bmc

Design, synthesis, and bioevaluation of benzamides: Novel acetylcholinesterase inhibitors with multi-functions on butylcholinesterase, Aβ aggregation, and β-secretase

Da-Yong Peng †, Qi Sun †, Xiao-Lei Zhu †, Hong-Yan Lin, Qiong Chen, Ning-Xi Yu, Wen-Chao Yang *, Guang-Fu Yang *

Key Laboratory of Pesticide & Chemical Biology, College of Chemistry, Ministry of Education, Central China Normal University, Wuhan 430079, PR China

ARTICLE INFO

Article history:
Received 6 August 2012
Revised 8 September 2012
Accepted 10 September 2012
Available online 17 September 2012

Keywords:
Acetylcholinesterase
Alzheimer's disease
Benzamide
Structure-based design

ABSTRACT

Alzheimer's disease (AD) is a multifactorial syndrome with several target proteins contributing to its etiology. In this study, we conducted a structure-based design and successfully produced a series of new multi-site AChE inhibitors with a novel framework. Compound **2e**, characterized by a central benzamide moiety linked to an isoquinoline at one side and acetophenone at the other, was the most potent candidate with K_i of 6.47 nM against human AChE. Particularly, it showed simultaneous inhibitory effects against BChE, Aβ aggregation, and β-secretase. We therefore conclude that compound **2e** is a very promising multi-function lead for the treatment of AD.

© 2012 Elsevier Ltd. All rights reserved.

1. Introduction

As the most common type of dementia, neurodegenerative Alzheimer's disease (AD) is one of the leading causes of death worldwide. Despite decades of intensive study, the specific cause of AD remains enigmatic.[1] Most researchers support that several pathological phenomena are closely associated with AD lesions, such as a decrease of the neurotransmitter acetylcholine (ACh), formation of amyloid β-protein (Aβ) plaques, and abnormal post-translational modifications of tau protein to yield neurofibrillary tangles.[2–7] During the last twenty years, much effort has been aimed at developing strategies to reduce or clear the related AD pathological phenomena.[8,9] Based on the cholinergic hypothesis, two major strategies have been developed to control the ACh level.[10] One approach focuses on discovery of small molecule inhibitors as antagonists of acetylcholinesterase (AChE) that inhibit the breakdown of ACh while the other approach strives to discover small molecules to bind with ACh receptors as agonists.[3,11–13] To block the formation of amyloid plaques, two methods have been reported. One is the design of inhibitors of β-secretase or γ-secretase to decrease the generation of Aβ, or non-natural amino acid or transition metal complexes to block Aβ fibril formation.[2,14] The other tactic is to design antibodies or catalytic antibodies to bind and/or degrade Aβ.[14] In an effort to suppress the abnormal posttranslational modifications, for example, phosphorylation of tau protein, various attempts have been carried out, either to inhibit serine/threonine kinases which function as phosphorylating enzymes of tau protein, or to accelerate the dephosphorylation of hyper-phosphorylated tau protein. Although some of these strategies were invalidated due to severe side effects, several possible candidates have been advanced to clinical trials.

Tacrine was the first AChE inhibitor permitted by the FDA to enter the medical market. However, after a long period of using these AChE inhibitors to treat mild or moderate AD in clinical practice, a profile of adverse effects was gradually recognized, including increased rates of syncope, bradycardia, acute liver toxicity, and hip fracture in older adults. Most of the efforts in AChE inhibitor discovery concentrated on structural modification of the existing drugs or a combination of active substructures.[15–21] While the resulting compounds might suffer the risk of adverse effects due to the similarities in the scaffold, though some of the modified compounds showed much higher AChE-binding affinities.[16,19,21] Therefore, AChE inhibitors with novel scaffolds are urgently needed.

Abbreviations: AD, Alzheimer's disease; AChE, acetylcholinesterase; BChE, butylcholinesterase; ACh, acetylcholine; Aβ, amyloid-β; CAS, catalytic active site; PAS, peripheral active site; MD, molecular dynamic; SIE, solvated interaction energy; ATC, acetylthiocholine; MTDLs, multi-target-directed ligands; ESI-MS, electrospray ionisation mass spectrometry; DMF, dimethylformamide; DTNB, 5′, 5′-dithio-bis(2-nitrobenzoic acid); LGA, Lamarkian genetic algorithm; RESP, restrained electrostatic potential.

* Corresponding authors.
E-mail addresses: tomyang@mail.ccnu.edu.cn (W.-C. Yang), gfyang@mail.ccnu.edu.cn (G.-F. Yang).

† These authors contributed equally to this work.

0968-0896/$ - see front matter © 2012 Elsevier Ltd. All rights reserved.
http://dx.doi.org/10.1016/j.bmc.2012.09.016

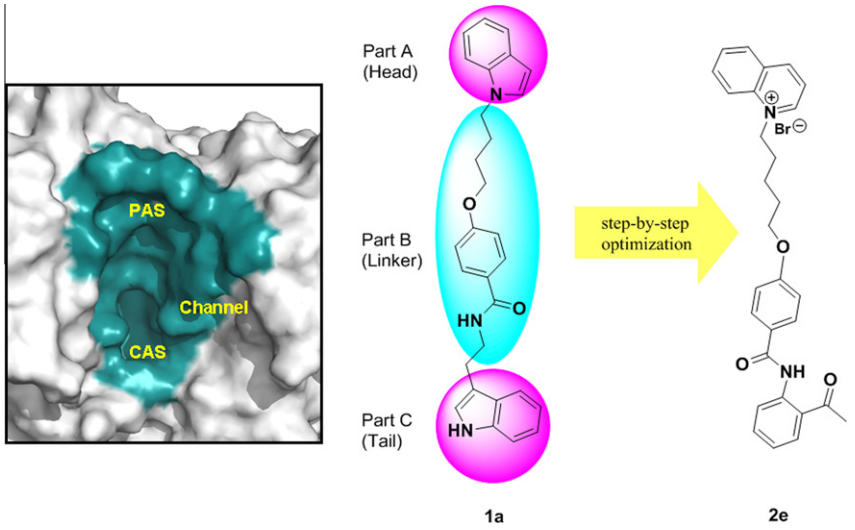

Figure 1. Molecular design strategy of lead compound **1a** and structural optimization leading to the discovery of compound **2e**. Left, the inhibitor-binding pocket of AChE consists of three subsites: catalytic active site (CAS), peripheral active site (PAS), and a narrow channel between the CAS and PAS.

Three dimensional structures of AChE from different species, including human, *Electrophorus electricus*, *Torpedo californica,* and mouse, have been determined in the past decade.[22,23] These structures revealed that there are two major subsites, the catalytic active site (CAS) and the peripheral active site (PAS), in the inhibitor-binding gorge-like pocket.[16,24] Recently, a narrow channel between the CAS and PAS was also identified as an additional binding site.[25] In addition, the gorge-like pocket is very rich in aromatic residues, especially in the PAS and CAS, such as residues Tyr72, Trp86, Tyr124, Trp286, Phe295, Tyr337, Tyr341 and Trp439. Based on these observations and some typical publications,[17,18,25,26] we proposed that an ideal AChE inhibitor should be composed of three structural units: an aromatic ring as the head to bind with the PAS, another aromatic ring as the tail to interact with the CAS region, and a linker to connect the head and tail. Taking into consideration that the indole moiety is an important aromatic ring with a broad spectrum of biological activity, hence we intentionally designed compound **1a** by introducing a *p*-hydroxybenzamide ring as a linker to connect the head and tail. The present paper describes our step-by-step optimization of this novel scaffold which culminated in development of compound **2e**, characterized by a central benzamide moiety linked to an isoquinoline at one side and acetophenone at the other, with a K_i value of 6.47 nM against human AChE (Fig. 1). The inhibitory effects of **2e** on human butylcholinesterase (BChE), Aβ aggregation and β-secretase indicated that this compound could be a multifunctional lead candidate for Alzheimer's disease therapy.

2. Results and discussion

2.1. Chemistry

As shown in Scheme 1, 3-aminoethylindole reacted with 4-hydroxybenzoic acid to afford the key intermediate **4**,

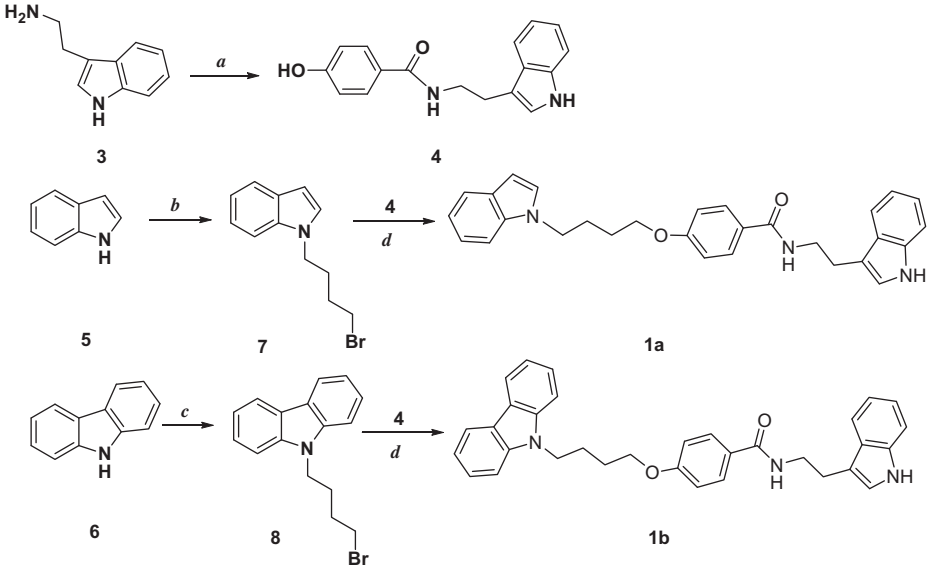

Scheme 1. Synthesis of compounds **1a** and **1b**. Reagents and conditions: (*a*) dicyclohexylcarbodiimide, *p*-hydroxybenzoic acid, THF, ice bath; (*b*), $Br(CH_2)_4Br$, KOH, DMF; (*c*) $Br(CH_2)_4Br$, NaOH; TBAB, benzene; (*d*) K_2CO_3, acetone, reflux.

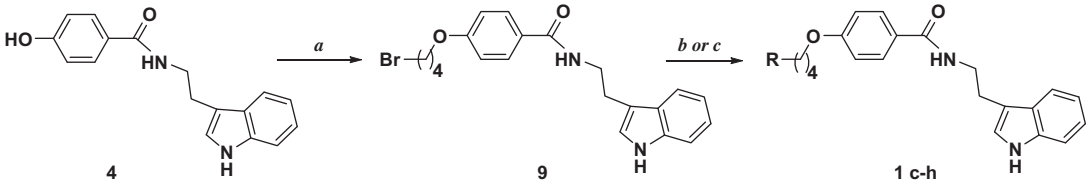

Scheme 2. Synthesis of compounds **1c**–**h**. Reagents and conditions: (*a*) $Br(CH_2)_4Br$, K_2CO_3, acetone, reflux; (*b*) substituted phenol, K_2CO_3, acetone, reflux; (*c*) *N*,*N*-dimethylaminopyridine or quinoline, CH_3CN, reflux.

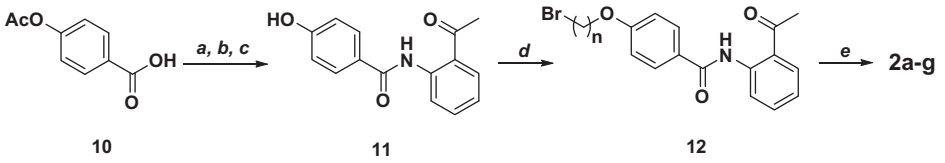

Scheme 3. Synthesis of compounds **2a**–**g**. Reagents and conditions: (*a*) $SOCl_2$, DMF, reflux; (*b*) *o*-aminoacetophenone, CH_2Cl_2, ice bath; (*c*) NaOH, MeOH/H_2O, rt; (*d*) $Br(CH_2)nBr$, K_2CO_3, acetone, reflux; (*e*) quinoline, isoquinoline, or pyridine, CH_3CN, reflux.

N-(2-(1*H*-indol-3-yl)ethyl)-4-hydroxybenzamide. Meanwhile, N-alkylation of indole or carbazole by 1,4-dibromobutane produced intermediates **7** and **8** according to the existing method,[27,28] which were then reacted with **4** to afford compounds **1a**–**b**. Alternatively, as depicted in Scheme 2, compounds **1c**–**h** were prepared in moderate yields through a two-step procedure by using *N*-(2-(1*H*-indol-3-yl)ethyl)-4-hydroxybenzamide **4** as the starting material.[29] Finally, compounds **2a**–**g** were smoothly prepared in good yields (75–85%) from 4-acetoxybenzoic acid by a multiple-step synthetic route as displayed in Scheme 3. The structures of all the target compounds were characterized by ^1H NMR, ^{13}C NMR, elemental analysis, and MS spectra.

2.2. Lead design and optimization

To obtain a lead compound that can fit well into the active site and efficiently inhibit the AChE, we undertook a structural analysis. A remarkable characteristic of the active site gorge is that more than ten aromatic residues comprise a substantial portion of the surface of the gorge, such as Trp286, Phe297, Phe295, Phe338, Tyr124 and Tyr 72 in the PAS; Trp86, Tyr337 and Trp439 in the CAS; and Tyr341 in the narrow linking channel. More aromatic residues may indirectly affect the configuration of the active site gorge.[30,31] Optimization of the π–π stacking interactions between inhibitor and aromatic residues in the binding pocket can greatly improve the binding affinity of inhibitors.[32,33] Bearing this consideration in mind, we initially designed a multi-site inhibitor which can form favorable π–π stacking interactions in all three subsites of the gorge. As a typical aromatic heterocyclic compound, the indole ring was chosen as the moiety to bind both the PAS and CAS due to its unique broad spectrum biological activities. To form a stacking interaction in the channel area, a simple benzamide was introduced to link the two indole rings, thus generating the compound **1a** (Scheme 1). Corresponding to the three sites (PAS, linker or CAS) of the active site gorge, the structure of this lead compound was also divided into three parts designated as part A, part B and part C (Fig. 1). When we assessed the inhibitory potency of **1a** on recombinant human AChE in comparison with tacrine and

Table 1
Structures of compounds **1a**–**h** and their inhibition constants (K_i) against human AChE

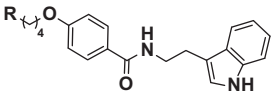

Compound	R	K_i (nM)	Compound	R	K_i (nM)
Tacrine	—	32.12	**1d**	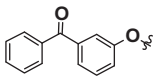	>10,000
Galanthamine	—	61.96	**1e**	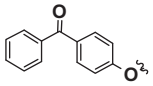	>10,000
1a		>10,000	**1f**	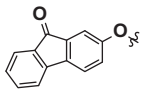	>10,000
1b	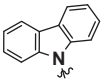	1437.00	**1g**	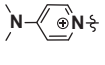	197.78
1c		>10,000	**1h**		123.73

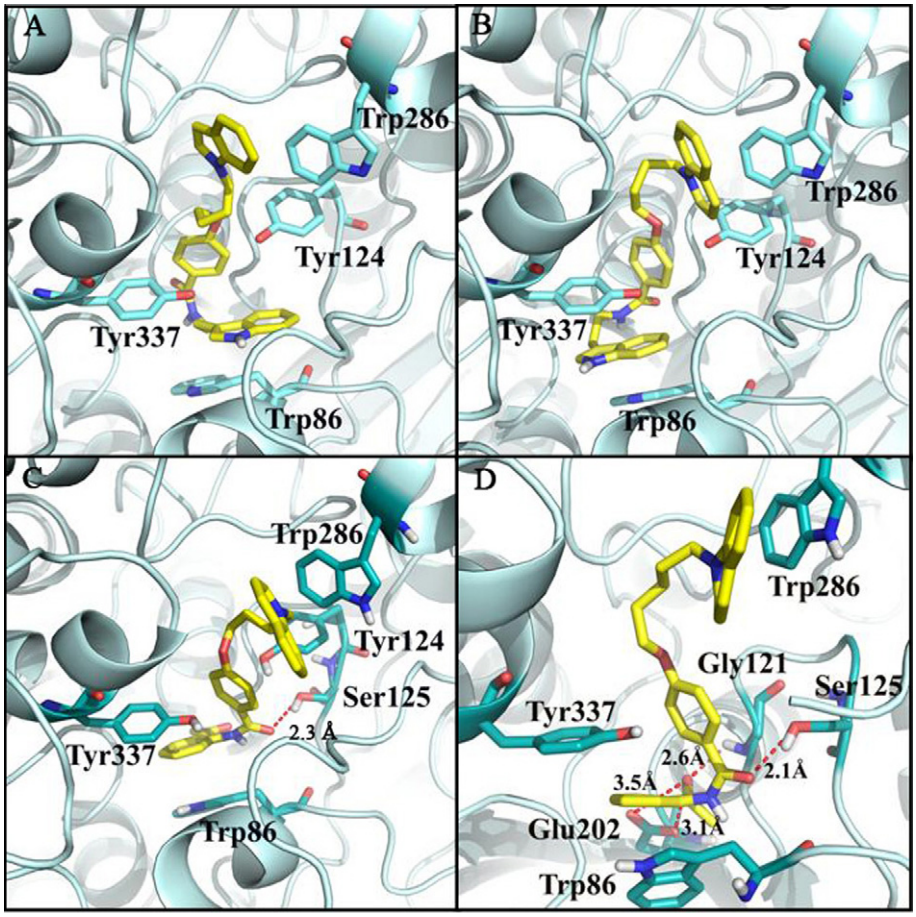

Figure 2. The simulated binding modes of four representative compounds. (A) Part A of compound **1a** formed π–π stacking interaction with Trp286 in PAS, while the part C of compound **1a** formed π–π stacking interaction with Trp86 in CAS. (B) The potency of compound **1h** is greatly improved due to the ionic interaction between the quinoline and the surrounding negatively charged residues in PAS. (C) The potency of compound **2a** is further improved due to the formation of the hydrogen bond (2.3 Å) between amide oxygen of the bridge and Ser125. (D) compound **2e** was obtained by replacing the four-methylene linker with a five-methylene linker, its potency was improved significantly due to the formation of two hydrogen bonds (3.1 and 3.5 Å) between the carbonyl oxygen of acetophenone and Glu202, and a hydrogen bond (2.6 Å) between the carbonyl oxygen of acetophenone and Gly121.

galanthamine (Table 1), the lead compound showed negligible inhibition against human AChE. Molecular docking and molecular dynamic (MD) simulations indicated that part A of **1a** favorably interacted with the PAS and part C interacted with the CAS. As indicated in Figure 2A (AChE PDB ID, 1b41), the indole ring in part A of **1a** stacked with Try286, the benzene ring of part B with Try337, and the indole ring of part C formed a strong stacking interaction with Trp86. However, compound **1a** did not show high binding affinity may because the π-π stacking interactions in the PAS were not optimized.

To enhance the stacking interaction between part A and PAS, we designed compounds **1b–f**, in which the part A indole ring was replaced by a series of aromatic rings such as carbazole and benzophenone (Table 1). Among these compounds, **1b** displayed improved potency with a K_i value of 1437.00 nM against human AChE, whereas **1c–f** showed no improvement in potency compared to compound **1a**.

We observed that the PAS region is also rich in negatively charged residues. Generally, the ionic interactions are stronger than the π–π stacking interactions. We reasoned that if the part A indole ring of **1a** was replaced with a positively charged quaternary nitrogen, the resultant compounds **1g** and **1h** should bind with the PAS pocket through ionic interactions as well as π–π stacking. As expected, compounds **1g** and **1h** did show significantly improved potency with K_i values of 197.78 and 123.73 nM, respectively, about 70- and 100-fold better than **1a**. The binding model of compound **1h** is illustrated in Figure 2B.

Hydrogen bonding makes a great contribution to ligand-receptor interactions, so we tried to introduce residues that would serve as hydrogen bond acceptors into part C of the ligand with the aim of forming new interactions in the CAS pocket in addition to the π–π stacking interactions. To avoid significantly changing the binding conformation of compound **1h**, we replaced the indole ring of part C with acetophenone to yield compound **2a** (Fig. 3). Acetophenone was chosen here since it is a single aromatic ring with a simple hydrogen bond acceptor. The potency of compound **2a** was improved in a promising manner, displaying a K_i value of 53.34 nM against human AChE. The aim of introducing acetophenone was to form a hydrogen bond between the carbonyl oxygen of acetophenone and the surrounding residues in the CAS. However, as depicted in Figure 2C, the carbonyl oxygen of the benzamide rather than that of the acetophenone formed a strong hydrogen bond (2.3 Å) with Ser125. As expected, the binding conformation of compound **2a** did not significantly change compared to that of compound **1h**.

After analyzing the interaction between compound **2a** and AChE, we noticed that there are some important residues surrounding the acetophenone of compound **2a**, such as Gly121, Glu202, Tyr337 and Tyr341. We speculated that adjusting the length of the linker would permit the carbonyl oxygen of

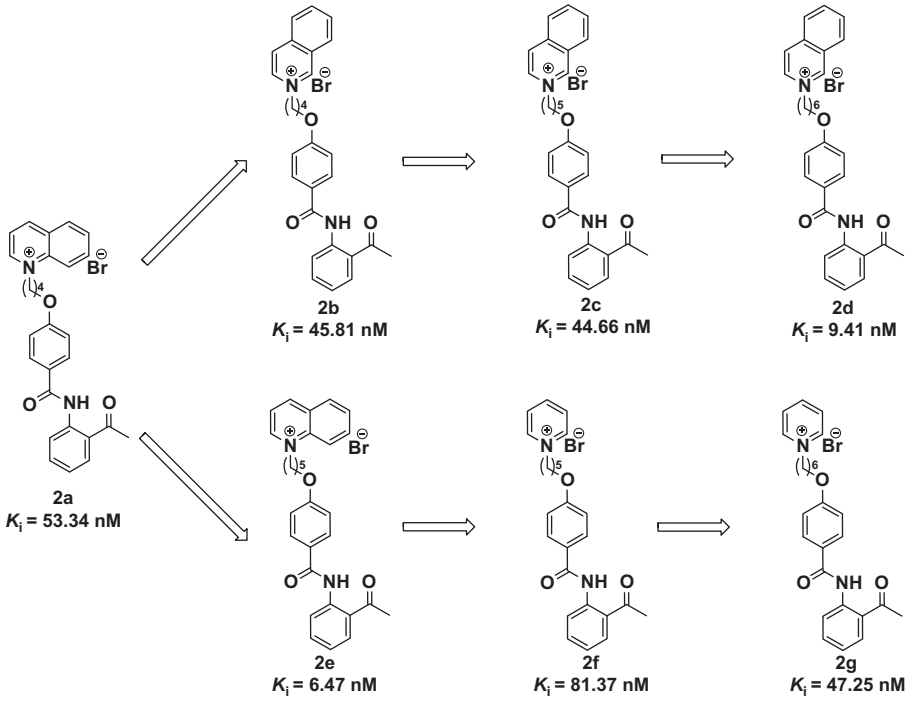

Figure 3. Structures of compounds **2a**–**g**, and their inhibition constants (K_i) against human AChE.

Table 2
The detailed values and correlation between the experimental and calculated binding free energies (kcal/mol) of compounds **2a**–**g**

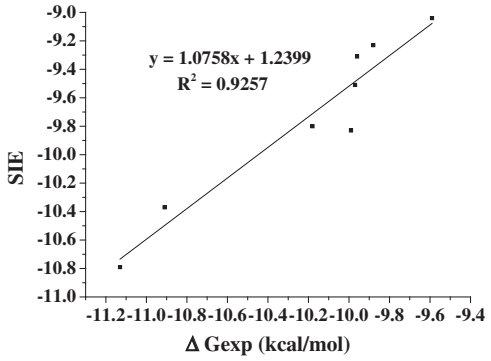

	Tacrine	2a	2b	2c	2d	2e	2f	2g
K_i (nM)	32.12	53.34	45.81	44.66	9.41	6.47	87.37	47.25
$\triangle G_{exp}$	−10.18	−9.88	−9.97	−9.99	−10.91	−11.13	−9.59	−9.96
SIE	−9.80	−9.23	−9.51	−9.83	−10.37	−10.79	−9.04	−9.31

acetophenone to form hydrogen bonding interactions with these residues. Therefore, we designed compounds **2b**–**g** with linkers of different lengths. We also substituted isoquinoline and pyridine in part A. As a result, compounds **2b** (K_i = 45.81 nM) and **2c** (K_i = 44.66 nM) showed slightly improved potency, but compound **2d**, whose linker contained six methylene units, was found to exhibit a much higher activity (K_i = 9.41 nM). Most promisingly, compound **2e** with a linker one carbon longer than in compound **2a** showed the highest inhibitory effects against human AChE with K_i value of 6.47 nM, about 7-fold improved potency than **2a** (K_i = 53.34 nM). However, further extending the linker resulted in the decrease of the potency. For example, compounds **2f** (K_i = 81.37 nM) and **2g** (K_i = 47.25 nM), whose linkers respectively contained five and six methylene units, showed much lower potency than compound **2e**. The lipophilicity and solubility of the new compounds were affected during the above structural evolution. However no obvious relationships were identified between these physicochemical properties and the practical inhibition potencies, because some compounds with lower solvability demonstrated better inhibition potency in our assay.

Compared with the original lead compound **1a**, compound **2e** showed 1500-fold improved potency against human AChE. As shown in Figure 2D based on molecular modeling, in addition to the π–π stacking interactions with Trp286 at PAS and Trp86 at

Table 3
Inhibitory activities and selectivities of compounds **1g–h**, **2a–g** on human AChE and BChE

Compounds	K_i (nM)		Selectivity AChE/BChE[a]	Relative selectivity[b]
	For AChE	For BChE		
Tacrine	32.12 ± 2.13	8.72 ± 2.13	0.27	1.00
Galanthamine	61.96 ± 5.63	192.47 ± 17.57	3.10	11.48
1g	198.00 ± 29.10	2360.00 ± 331.00	11.92	44.16
1h	124.00 ± 17.40	97.00 ± 10.20	0.79	2.91
2a	53.00± 7.82	166.00 ± 10.90	3.10	11.49
2b	46.00 ± 3.80	56.00 ± 6.70	1.22	4.52
2c	45.00± 5.70	82.00 ± 9.80	1.83	6.78
2d	9.40 ± 0.80	99.00 ± 2.80	10.53	39.00
2e	6.50 ± 0.90	55.00 ± 6.70	8.57	31.74
2f	81.00 ± 13.10	93.00 ± 11.10	1.06	3.92
2g	47.00 ± 3.80	66.00 ± 7.90	1.39	5.15

[a] Selectivity of inhibitor potency for AChE over BChE.
[b] Relative selectivity of inhibitor potency for AChE over BChE compared with selectivity of tacrine against AChE over BChE.

CAS, compound **2e** formed four hydrogen bonds with its surrounding residues in the binding pocket. The amide oxygen of the bridge formed a strong hydrogen bond with residue Ser125 with a distance of 2.1 Å , while the carbonyl oxygen of acetophenone formed two hydrogen bonds with Glu202 (3.1 and 3.5 Å) and a hydrogen bond with Gly121 (2.6 Å). These hydrogen bond interactions account for the molecular basis of the superior potency of **2e**.

In order to quantitatively study the structure–activity relationships of those new potent multi-site AChE inhibitors, solvated interaction energy (SIE) calculations were performed based on the molecular docking simulations, using tacrine as an internal reference. The SIE were obtained by calculations and experimental binding free energy (ΔG_{exp}) derived from the experimental data (Table 2). The calculated SIE for the inhibitors ranged from −9.04 to −10.79 kcal/mol, while the ΔG_{exp} ranged from −9.59 to −11.13 kcal/mol. Obviously, the order of the calculated SIE agreed qualitatively with that of the experimental binding free energies. More importantly, there was a good linear correlation ($r^2 = 0.93$) between the calculated SIE and the ΔG_{exp}, suggesting that our computational protocol used to guide the structural optimization of AChE inhibitors should be reliable.

2.3. Human BChE inhibition

In addition to AChE, BChE has now been recognized as another target due to its relevance to the occurrence, symptoms, progression and responses to treatment in AD. Solid experimental evidence has shown that the contribution of brain cholinesterase activity from AChE is much higher than that of BChE.[34] However, the relative proportions of AChE to BChE are dependent on the brain regions and the stage of disease progression in AD patients.[35] In addition, clinical results have indicated that BChE activity increases as AD progresses, which suggests that BChE may also play an important role in cholinergic dysfunction, particularly at the later stages of AD. In considering BChE as another important target for AD treatment, the administration of inhibitors with different AChE/BChE selectivity should be very useful as AD progresses. Therefore, we screened all the newly synthesized compounds against human BChE using tacrine and galanthamine as references. For the candidates with better activity against human AChE, their binding affinities for human BChE were assessed based on the inhibitory kinetics with acetylthiocholine (ATC) as substrate (Table 3). All the new compounds except **1g**, with nanomolar level activity, were less potent than tacrine for human BChE but more active than galanthamine. According to the inhibitory kinetic findings, the new cholinesterase inhibitors displayed various selectivities on human AChE and BChE. Particularly, the selectivity of compound **2d** decreased ~38-fold compared to that of tacrine, and it showed about ~10-fold better inhibitory activity against human AChE than against BChE. Another interesting point is that compound **2f** showed almost same inhibitory activity against both human AChE and BChE.

Table 4
Aβ aggregation and β-secretase inhibitory effects of compounds **2c–f**

Targets	IC_{50} (μM)				
	Curcumin	**2c**	**2d**	**2e**	**2f**
Aβ	10.4 ± 0.8	71 ± 3.2	50 ± 4.3	79 ± 4.7	>250
β-secretase	5.7 ± 1.2	>100	>100	85 ± 10.1	0.31 ± 0.11

2.4. Inhibition of Aβ aggregation

Recent explorations suggests that both AChE and BChE have been associated with other non-traditional functions in addition to their traditional regulation of ACh-mediated neurotransmission, including modulatory effects on the Aβ fibrillization, glial proliferation, β-APP expression, tau protein phosphorylation, inflammatory processes, and other pathological phenomena.[35] Various AChE inhibitors that interact with PAS of AChE have been demonstrated to block in vitro Aβ aggregation, reduce oxidative stress, and partially relieve the hyper-phosphorylation of tau protein.[21,36] Thus, AChE inhibitors or ChE inhibitors may contribute to AD treatment in ways other than those proposed by the cholinergic hypothesis. Discovery of new AChE inhibitors or multi-target-directed ligands (MTDLs) addressing distinct AD-relevant targets has been an active area in AD research.[7,16,18–20,37–41] We therefore tested the inhibitory activity of our newly synthesized multi-site AChE inhibitors against Aβ aggregation, using curcumin as a positive control.

The thioflavin T competition assay is a widely used fluorescent method to detect amyloid structures, particularly in the presence of AChE inhibitors. In parallel with the cholinesterase inhibition assay, all the new highly active AChE inhibitors were screened for their inhibitory activity on Aβ self-aggregation and tacrine was used as another reference. Tacrine showed around 12% inhibition rate in the crude screening, while some multi-site AChE inhibitors also showed significant inhibitory activity against Aβ self-aggregation. Based on screening with a single dosage of 100 μM, compounds **2c–f** with high inhibition percentages above 50% were identified for full kinetic characterization and their detailed IC_{50} values are listed in Table 4. All these new compounds exhibited limited activity toward Aβ self-aggregation, which needs further investigation in the future.

2.5. Inhibition of β-secretase

Due to its involvement in the proteolytic cleavage of amyloid precursor protein (APP) to Aβ, β-secretase has encouraged great interest as a therapeutic target for disease-modifying agents in AD.[42–45] Some dual binding site AChE inhibitors such as tacrine derivatives have been reported to exhibit β-secretase inhibitory activity.[46] Thus, the capability of newly synthesized compounds was firstly evaluated at a single concentration (100 μM) against β-secretase by fluorometric assay, followed by further kinetic characterization of promising candidates if their inhibition rates were no less than 50% percent at the screening concentration. As displayed in Table 4, compound **2e** showed modest potency against β-secretase, whereas compound **2f** revealed good potency against β-secretase with an IC_{50} value of 0.31 μM.

3. Conclusions

Tacrine and its derivatives have high inhibitory activity against AChE, but their severe toxicity limited their clinical application. In this work, non-tacrine based novel compounds as potent multi-site AChE inhibitors were successfully designed by a combination of computational simulations and experimental studies. In particular, compound **2e**, characterized by a central benzamide moiety linked to an isoquinoline at one side and acetophenone at the other, was identified as the most potent multi-site AChE inhibitor with a K_i value of 6.47 nM, about 4-fold and 1500-fold higher potency than tacrine and the original lead compound **1a**, respectively. Moreover, the inhibitory effects toward human BChE, Aβ aggregation, and β-secretase of some of the newly synthesized multi-site AChE inhibitors were also evaluated. Interestingly, compound **2e** also showed simultaneously inhibitory effects against BChE, Aβ aggregation, and β-secretase. In addition, compound **2f**, bearing a pyridinium functionality as the head for the binding of PAS pocket, was identified as an excellent β-secretase inhibitor with an IC_{50} value of 0.31 μM. In summary, due to the high potency towards not only AChE, but also other important targets associated with AD therapy, compound **2e** could be a promising multifunctional lead for the treatment of AD. For the requirement of entering the brain, further structural improvement and ideal formulation of these novel potent multi-functional inhibitors with lipophilic quaternary ammonium will be needed.

4. Materials and methods

Unless otherwise noted, all chemical reagents were commercially available and treated with standard methods before use. Solvents were dried in a routine way and redistilled before use. ^{1}H NMR and ^{1}C NMR spectra were recorded on a VARIAN Mercury-Plus 600 or 400 spectrometer in $CDCl_3$ or DMSO-d_6 with TMS as the internal reference. Mass spectral data were obtained on a ThermoFisher Mass platform DSQII by electrospray ionization (ESI-MS). Elemental analyses were performed on a Vario EL III elementary analysis instrument. Melting points were taken on a Buchi B-545 melting point apparatus and are uncorrected. All chemical yields are unoptimized and generally represent the result of a single experiment.

4.1. General procedure for *N*-(2-(1*H*-indol-3-yl)ethyl) hydroxybenzamide 4

To a mixture of *p*-hydroxybenzoic acid (6 mmol) in THF (50 mL), dicyclohexylcarbodiimide (6 mmol) was added at 0 °C with stirring for 1 h. Tryptamine (5 mmol) was then added and stirred further for 24 h at room temperature, followed by filtration. The crude product was purified by silica column chromatography using ethyl acetate/petroleum (V/V = 1/4) to give pure compounds in a yield of 71% as a white solid. mp 173–175 °C. MS (EI) *m*/*z*: 280.21 $(M)^+$. ^{1}H NMR (600 MHz, DMSO-d_6): δ 10.79 (s, 1H), 9.92 (s, 1H), 8.34 (t, *J* = 5.4 Hz, 1H), 7.72 (d, *J* = 8.4 Hz, 2H), 7.58 (d, *J* = 7.8 Hz, 1H), 7.34 (d, *J* = 7.8 Hz, 1H), 7.17 (s, 1H), 7.06 (t, *J* = 7.2 Hz, 1H), 6.98 (t, *J* = 7.2 Hz, 1H), 6.79 (d, *J* = 8.4 Hz, 2H), 3.51 (dd, *J* = 13.8, 6.6 Hz, 2H), 2.92 (t, *J* = 7.8 Hz, 2H).

4.2. General synthesis of intermediate 7

To a stirred solution of 6.06 g (30 mmol) of 1,4-dibromobutane in 50 mL of DMF was added 1.17 g (10 mmol) of indole and 0.57 g (10 mmol) of ground KOH powder. The mixture was stirred overnight. Water (100 mL) was added and the product was extracted into ether (3 × 50 mL). The ether extracts were washed with H_2O, dried over $MgSO_4$, and evaporated. The residue was chromatographed on silica gel using petroleum ether to give 1.8 g intermediate **7** (oil). ^{1}H NMR (600 MHz, DMSO-d_6): δ 7.55 (t, *J* = 9.6 Hz, 1H), 7.46–7.36 (m, 1H), 7.33 (d, *J* = 7.8 Hz, 1H), 7.14–7.04 (m, 1H), 7.00 (d, *J* = 6.0 Hz, 1H), 6.43 (d, *J* = 9.0 Hz, 1H). 4.21 (t, *J* = 6.0 Hz, 2H), 3.53 (t, *J* = 7.2 Hz, 2H), 1.93–1.81 (m, 2H), 1.79–1.67 (m, 2H).

4.3. General synthesis of intermediate 8

A mixture of 59.1 g (237.7 mmol) of 1,4-dibromobutane, 1 g of triethylbenzylammonium chloride, 5.16 g (30.86 mmol) of carbazole, 50 ml of aqueous 50% sodium hydroxide, and 50 mL benzene was stirred at 40–50 °C for 6 h. The organic layer was separated, and the aqueous layer was extracted three times with chloroform (3 × 50 mL). The combined organic layer was washed three times with water (3 × 50 mL) and dried over Na_2SO_4. The organic solvent was distilled by vacuum distillation, and then chromatographed on silica gel using petroleum ether to give 5.8 g compound **8**. Yield 62%; mp 101–103 °C. ^{1}H NMR (600 MHz, $CDCl_3$): δ 8.11 (d, *J* = 7.8 Hz, 2H), 7.47 (t, *J* = 7.8 Hz, 2H), 7.41 (t, *J* = 8.4 Hz, 2H), 7.28–7.20 (m, 2H), 4.36 (t, *J* = 7.2 Hz, 2H), 3.38 (t, *J* = 6.6 Hz, 2H), 2.11–2.02 (m, 2H), 1.95–1.88 (m, 2H).

4.4. General procedure for the synthesis of compounds 1a and 1b

Compound **4** (1 mmol), compound **7** or **8** (1.1 mmol), and potassium carbonate (2.2 mmol) were mixed together and stirred in dry acetone (50 mL) under reflux for 24 h. The solution was evaporated in vacuum and purified by column chromatography using gradient elution of petroleum ether/ethyl acetate (V/V = 2/3) to afford the product as **1a** or **1b**.

4.4.1. 4-(4-(1H-indol-1-yl)butoxy)-*N*-(2-(1H-indol-3-yl)ethyl)benzamide (1a)

White solid; yield 34%; mp 57–59 °C; ^{1}H NMR (600 MHz, DMSO-d_6): δ 10.80 (s, 1H), 8.43 (s, 1H), 7.80 (d, *J* = 8.4 Hz, 2H), 7.58 (d, *J* = 7.8 Hz, 1H), 7.54 (d, *J* = 7.8 Hz, 1H), 7.49 (d, *J* = 8.4 Hz, 1H), 7.39 (d, *J* = 2.4 Hz, 1H), 7.34 (d, *J* = 8.4 Hz, 1H), 7.17 (s, 1H), 7.13 (t, *J* = 7.8 Hz, 1H), 7.06 (t, *J* = 7.2 Hz, 1H), 7.01 (t, *J* = 7.2 Hz, 1H), 6.98 (d, *J* = 7.8 Hz, 1H), 6.95 (d, *J* = 8.4 Hz, 2H), 6.43 (s, 1H), 4.25 (t, *J* = 6.6 Hz, 2H), 4.02 (t, *J* = 6.0 Hz, 2H), 3.54–3.49 (m, 2H), 2.93 (t, *J* = 7.2 Hz, 2H), 1.93–1.88 (m, 2H), 1.72–1.65 (m, 2H). ^{13}C NMR (100 MHz, DMSO-d_6): δ 165.64, 160.77, 136.27, 135.66, 128.94, 128.56, 128.12, 127.32, 126.86, 122.58, 120.96, 120.44, 118.86, 118.34, 118.23, 113.86, 112.01, 111.39, 109.77, 100.47, 67.22, 45.11, 40.17, 26.55, 26.01, 25.33. MS (EI) *m*/*z*: 451.31 $(M)^+$. Anal. Calcd for $C_{29}H_{29}N_3O_2$: C, 77.13; H, 6.47; N, 9.31. Found: C, 77.04; H, 6.65; N, 9.35.

4.4.2. *N*-(2-(1*H*-indol-3-yl)ethyl)-4-(4-(9*H*-carbazol-9-yl)butoxy) benzamide (1b)

White solid; yield 41%; mp 131–132 °C; ^{1}H NMR (600 MHz, DMSO-d_6): δ 10.81 (s, 1H), 8.45 (s, 1H), 8.16 (d, J = 7.8 Hz, 2H), 7.79 (d, J = 8.4 Hz, 2H), 7.64 (d, J = 8.4 Hz, 2H), 7.57 (d, J = 7.8 Hz, 1H), 7.46 (t, J = 7.8 Hz, 2H), 7.33 (d, J = 7.8 Hz, 1H), 7.20 (t, J = 7.2 Hz, 2H), 7.17 (s, 1H), 7.06 (t, J = 7.2 Hz, 1H), 7.01–6.96 (m, 1H), 6.95 (t, J = 7.8 Hz, 2H), 4.49 (t, J = 6.6 Hz, 2H), 4.03 (t, J = 6.0 Hz, 2H), 3.61–3.51 (m, 2H), 2.92 (t, J = 7.2 Hz, 2H), 1.98–1.89 (m, 2H), 1.80–1.73 (m, 2H). ^{13}C NMR (100 MHz, DMSO-d_6): δ 165.65, 160.78, 139.97, 136.28, 128.95, 127.33, 126.87, 125.69, 122.59, 122.06, 120.95, 120.29, 118.70, 118.36, 118.24, 113.85, 112.02, 111.40, 109.26, 67.32, 41.87, 40.18 ,26.24, 25.34, 25.23. MS (EI) m/z: 501.06 (M)$^+$. Anal. Calcd for $C_{33}H_{31}N_3O_2$: C, 79.01; H, 6.23; N, 8.38. Found: C, 78.81; H, 6.36; N, 8.14.

4.5. General procedure for *N*-(2-(1*H*-indol-3-yl)ethyl)-(4-bromobutoxy) benzamide 9

A mixture of 1,4-dibromoalkane (30 mmol), compound **4** (10 mmol), potassium carbonate (20 mmol) and a catalytic amount of KI in 30 mL of acetone was stirred at 65 °C for 3 days. When the reaction was completed, as monitored by TLC detection, the solution was filtered. After solvent evaporation and purification by column chromatography using petroleum ether/CH_2Cl_2 (V/V = 1/0 to 2/3) for gradient elution, the final product was obtained in a yield of 65% as a white solid. mp 111–113 °C. MS (EI) m/z: 414.25 (M)$^+$. ^{1}H NMR (600 MHz, DMSO-d_6): δ 10.81 (s, 1H), 8.46 (s, 1H), 7.82 (d, J = 8.4 Hz, 2H), 7.58 (d, J = 7.8 Hz, 1H), 7.34 (d, J = 8.4 Hz, 1H), 7.17 (s, 1H), 7.06 (t, J = 7.2 Hz, 1H), 7.01–6.95 (m, 3H), 4.06 (t, J = 6.0 Hz, 2H), 3.62 (t, J = 6.6 Hz, 2H), 3.52 (dd, J = 13.8, 6.6 Hz, 2H), 2.93 (t, J = 7.2 Hz, 2H), 2.01–1.91(m, 2H), 1.89–1.81 (m, 2H).

4.6. General procedure for 4-hydroxyl benzoyl aromatic amine (11)

To a suspension of 4-acetoxybenzoic acid (50 mmol) and $SOCl_2$ (20 ml), DMF (0.5 ml) was added dropwise as catalyst. After stirring for a few minutes at room temperature, the solution became clear and was then heated at reflux for 2 h. After evaporating under reduced pressure, the solution was added dropwise to the mixture of *o*-aminoacetophenone (45 mmol), NEt_3 (100 mmol) and anhydrous CH_2Cl_2 (60 mL) in an ice bath. The reaction was continuously stirred at room temperature overnight. The solid was obtained by evaporation under reduced pressure and dissolved in MeOH/H_2O (V/V = 1/1, 100 ml). Later, the reaction mixture was stirred at room temperature for another 2 h after addition of NaOH (100 mmol). When the reaction was completed, as indicated by TLC detection, the pH was adjusted to 6.0 with 1 M HCl. Finally, the precipitate was filtered and washed by water, and then was redissolved in EtOAc and evaporated under reduced pressure to give the product in a yield of 81% as a white solid. mp 185–187 °C. MS (EI) m/z: 255.08 (M)$^+$. ^{1}H NMR (600 MHz, DMSO-d_6): δ 12.30 (s, 1H), 10.27 (s, 1H), 8.68 (d, J = 8.4 Hz, 1H), 8.11 (d, J = 7.8 Hz, 1H), 7.85 (d, J = 7.8 Hz, 2H), 7.66 (t, J = 7.8 Hz, 1H), 7.23 (t, J = 7.2 Hz, 1H), 6.94 (d, J = 8.4 Hz, 2H), 2.70 (s, 3H).

4.7. General procedure for 4-(ω-bromobutoxy) benzoyl aromatic amine 12

A mixture of α,ω-dibromoalkane (30 mmol), compound **11** (10 mmol), potassium carbonate (20 mmol) and a catalytic amount of KI in 30 mL of acetone was stirred at 65 °C for 3 days. The precipitate was filtered and evaporated, and further purified by column chromatography using gradient elution with petroleum ether/EtOAc (V/V = 1/0 to 2/3) to give pure products as **12a–c**.

4.7.1. N-(2-acetylphenyl)-4-(4-bromobutoxy)benzamide (12a)

White solid; yield 85%; mp 84–86 °C. MS (EI) m/z: 389.06 (M)$^+$. ^{1}H NMR (600 MHz, DMSO-d_6): δ 12.33 (s, 1H), 8.67 (d, J = 8.4 Hz, 1H), 8.11 (d, J = 7.8 Hz, 1H), 7.93 (d, J = 8.4 Hz, 2H), 7.67 (t, J = 7.8 Hz, 1H), 7.25 (t, J = 7.2 Hz, 1H), 7.14 (d, J = 8.4 Hz, 2H), 4.12 (t, J = 6.0 Hz, 2H), 3.63 (t, J = 6.6 Hz, 2H), 2.70 (s, 3H), 2.03–1.95 (m, 2H), 1.92–1.82 (m, 2H).

4.7.2. *N*-(2-acetylphenyl)-4-((5-bromopentyl)oxy)benzamide (12b)

White solid; yield, 83%. mp 92–94 °C. MS (EI) m/z: 403.19 (M)$^+$. ^{1}H NMR (600 MHz, DMSO-d_6) δ 12.30 (s, 1H), 10.27 (s, 1H), 8.68 (d, J = 8.4 Hz, 1H), 8.11 (d, J = 7.8 Hz, 1H), 7.85 (d, J = 7.8 Hz, 2H), 7.66 (t, J = 7.8 Hz, 1H), 7.23 (t, J = 7.2 Hz, 1H), 6.94 (d, J = 8.4 Hz, 2H), 4.07 (t, J = 7.2 Hz, 2H), 3.61 (t, J = 6.0 Hz, 2H), 2.70 (s, 3H), 2.18–2.08 (m, 2H), 1.88–1.79 (m, 2H), 1.56–1.48 (m, 2H).

4.7.3. *N*-(2-acetylphenyl)-4-((6-bromohexyl)oxy)benzamide (12c)

White solid; yield 83%; mp 92–94 °C. MS (EI) m/z: 403.19 (M)$^+$. ^{1}H NMR (600 MHz, DMSO-d_6): δ 12.33 (s, 1H), 8.67 (d, J = 8.4 Hz, 1H), 8.11 (d, J = 7.8 Hz, 1H), 7.93 (d, J = 8.4 Hz, 2H), 7.67 (t, J = 7.8 Hz, 1H), 7.25 (t, J = 7.8 Hz, 1H), 7.13 (d, J = 8.4 Hz, 2H), 4.07 (t, J = 6.6 Hz, 2H), 3.55 (t, J = 6.6 Hz, 2H), 2.70 (s, 3H), 1.89–1.80 (m, 2H), 1.80–1.71 (m, 2H), 1.48–1.44 (m, 4H).

4.8. General procedure for the syntheses of compounds 1c–h and 2a–g

Compounds **9** (1 mmol), corresponding phenol derivatives (1.1 mmol), and potassium carbonate (2.2 mmol) were mixed together and stirred in dry acetone (30 mL) under reflux for 24 h. The solution was evaporated in vacuum and purified by column chromatography using gradient elution of petroleum ether/ethyl acetate (V/V = 2/3) to afford the products as **1c–f**. Compounds **9** and **12a–c** (1 mmol) and corresponding pyridine derivatives (10 mmol) were mixed together and heated to reflux in dry acetonitrile (30 mL) for 24 h. Then the solvent was evaporated in vacuum and the product was purified by column chromatography using gradient elution of CH_2Cl_2/methanol (V/V = 10/3) to give the products as **1g–h** and **2a–g**.

4.8.1. *N*-(2-(1*H*-indol-3-yl)ethyl)-4-(4-((9*H*-carbazol-4-yl)oxy) butoxy)benzamide(1c)

White solid; yield 28%; mp 160–162 °C; ^{1}H NMR (600 MHz, DMSO-d_6): δ 11.26 (s, 1H), 10.82 (s, 1H), 8.48 (t, J = 5.4 Hz, 1H), 8.14 (d, J = 7.8 Hz, 1H), 7.83 (d, J = 8.4 Hz, 2H), 7.59 (d, J = 7.8 Hz, 1H), 7.45 (d, J = 8.4 Hz, 1H), 7.36–7.26 (m, 3H), 7.18 (s, 1H), 7.11 (t, J = 7.2 Hz, 1H), 7.09–7.04 (m, 2H), 7.02 (d, J = 8.4 Hz, 2H), 6.98 (t, J = 7.2 Hz, 1H), 6.71 (d, J = 7.8 Hz, 1H), 4.28 (d, J = 5.4 Hz, 2H), 4.20 (d, J = 6.0 Hz, 2H), 3.54–3.49 (m, 2H), 2.94 (t, J = 7.2 Hz, 2H), 2.12–2.02 (m, 4H). ^{13}C NMR (100 MHz, DMSO-d_6): δ 165.65, 160.83, 154.97, 141.13, 138.95, 136.27, 128.99, 127.33, 126.85, 126.54, 124.54, 122.60, 122.17, 121.77, 120.95, 118.66, 118.36, 118.25, 113.94, 112.02, 111.44, 110.45, 103.82, 100.40, 67.36, 67.10, 40.19, 25.73, 25.66, 25.36. MS (EI) m/z: 517.19 (M)$^+$. Anal. Calcd for $C_{33}H_{31}N_3O_3$: C, 76.57; H, 6.04; N, 8.12. Found: C, 76.41; H, 6.11; N, 8.33.

4.8.2. *N*-(2-(1*H*-indol-3-yl)ethyl)-4-(4-(3-benzoylphenoxy) butoxy)benzamide (1d)

White solid; yield 38%; mp 117–119 °C; ^{1}H NMR (600 MHz, DMSO-d_6): δ 10.83 (s, 1H), 8.49 (s, 1H), 7.83 (d, J = 8.4 Hz, 2H), 7.75 (d, J = 7.2 Hz, 2H), 7.69 (t, J = 7.2 Hz, 1H), 7.61–7.64 (m, 3H), 7.48 (t, J = 7.8 Hz, 1H), 7.34 (d, J = 8.4 Hz, 1H), 7.29–7.24 (m, 3H), 7.18 (s, 1H), 7.07 (t, J = 7.2 Hz, 1H), 7.01–6.96 (m, 3H), 4.12 (t,

J = 6.6 Hz, 2H), 3.55–3.49 (m, 2H), 3.17 (t, J = 5.4 Hz, 2H), 2.94 (t, J = 7.2 Hz, 2H), 1.96–1.85 (m, 4H). ^{13}C NMR (150 MHz, DMSO-d_6): δ 195.60, 165.77, 160.88, 158.61, 138.43, 137.06, 136.34, 132.72, 129.71, 129.66, 129.04, 128.56, 127.39, 126.90, 122.63, 122.18, 121.00, 119.07, 118.41, 118.30, 114.80, 113.90, 112.09, 111.45, 67.40, 67.33, 40.27, 25.39, 25.37. MS (EI) m/z: 532.06 $(M)^+$. Anal. Calcd for $C_{34}H_{32}N_2O_4$: C, 76.67; H, 6.06; N, 5.26. Found: C, 76.70; H, 5.77; N, 5.19.

4.8.3. *N*-(2-(1*H*-indol-3-yl)ethyl)-4-(4-(4-benzoylphenoxy) butoxy)benzamide (1e)

White solid; yield 31%; mp 134–136 °C; ^{1}H NMR (600 MHz, DMSO-d_6): δ 10.82 (s, 1H), 8.47 (s, 1H), 7.82 (d, J = 8.4 Hz, 2H), 7.75 (d, J = 8.4 Hz, 2H), 7.69 (d, J = 7.8 Hz, 2H), 7.67–7.63 (m, 1H), 7.61–7.51 (m, 3H), 7.34 (d, J = 7.8 Hz, 1H), 7.17 (s, 1H), 7.10 (d, J = 8.4 Hz, 2H), 7.09–7.04 (m, 1H), 7.03–6.94 (m, 3H), 4.17 (t, J = 6.6 Hz 2H), 4.11 (t, J = 7.2 Hz,2H), 3.54–3.49 (m, 2H), 2.93 (t, J = 7.2 Hz, 2H), 1.95–1.88 (m, 4H). ^{13}C NMR (100 MHz, DMSO-d_6): δ 194.43, 165.61, 162.39, 160.80,137.80, 136.25, 132.22,132.07, 129.26, 128.96, 128.44, 127.30, 126.85, 122.59, 120.92, 118.33, 118.22, 114.33, 113.89, 111.99, 111.38, 67.58, 67.27, 40.16, 25.32, 25.28. MS (EI) m/z: 532.26 $(M)^+$. Anal. Calcd for $C_{34}H_{32}N_2O_4$: C, 76.67; H, 6.06; N, 5.26. Found: C, 76.70; H, 5.77; N, 5.19.

4.8.4. *N*-(2-(1*H*-indol-3-yl)ethyl)-4-(4-((9-oxo-9*H*-fluoren-2-yl) oxy)butoxy)benzamide (1f)

Orange solid; yield 27%; mp 153–155 °C; ^{1}H NMR (600 MHz, DMSO-d_6): δ 10.82 (s, 1H), 8.47 (t, J = 5.4 Hz, 1H), 7.83 (d, J = 8.4 Hz, 2H), 7.71–7.66 (m, 2H), 7.61–7.53 (m, 3H), 7.34 (d, J = 8.4 Hz, 1H), 7.28 (t, J = 7.2 Hz, 1H), 7.20–7.12 (m, 3H), 7.07 (t, J = 7.2 Hz, 1H), 7.03–6.94 (m, 3H), 4.15 (t, J = 7.2 Hz, 2H), 4.11 (t, J = 6.6 Hz, 2H), 3.54–3.49 (m, 2H), 2.94 (t, J = 7.8 Hz, 2H), 1.94–1.85 (m, 4H). ^{13}C NMR (100 MHz, DMSO-d_6): δ 192.97, 165.72, 160.85, 159.89, 144.39, 136.31, 135.30, 135.06, 133.45, 128.99, 128.055, 127.35, 126.88, 123.85, 122.60, 122.20, 120.96, 120.63, 120.23, 118.27, 113.88, 112.06, 111.42, 109.78, 67.72, 67.27, 40.23, 25.39, 25.32. MS (EI) m/z: 530.18 $(M)^+$. Anal. Calcd for $C_{34}H_{30}N_2O_4$: C, 76.96; H, 5.70; N, 5.28. Found: C, 76.66; H, 5.70; N, 5.15.

4.8.5. 1-(4-(4-((2-(1*H*-indol-3-yl)ethyl)carbamoyl)phenoxy) butyl)-4-(dimethylamino)pyridin-1-ium bromide(1g)

White solid; yield 79%; mp 101–103 °C. ^{1}H NMR (600 MHz, DMSO-d_6): δ 10.83 (s, 1H), 8.48 (s, 1H), 8.34 (d, J = 7.2 Hz, 2H), 7.83 (d, J = 8.5 Hz, 2H), 7.58 (d, J = 7.8 Hz, 1H), 7.34 (d, J = 8.0 Hz, 1H), 7.17 (s, 1H), 7.09–7.02 (m, 3H), 7.00–6.94 (m, 3H), 4.25 (t, J = 7.2 Hz, 2H), 4.05 (t, J = 6.0 Hz, 2H), 3.55–3.49 (m, 2H), 3.18 (s, 6H), 2.93 (t, J = 9.6 Hz, 2H), 1.97–1.89 (m, 2H), 1.75–1.66 (m, 2H). ^{13}C NMR (100 MHz, DMSO-d_6): δ 165.54, 160.58, 155.76, 141.94, 136.20, 128.93, 127.26, 122.54, 120.87, 118.30, 118.17, 113.88, 111.94, 111.36, 107.67, 66.95, 56.23, 40.28, 39.69, 27.10, 25.83, 25.13. MS (EI) m/z: 457.2 $(M\text{-}Br)^+$. Anal. Calcd For $C_{28}H_{33}BrN_4O_2$: C, 62.57; H, 6.19; N, 10.42. Found: C, 62.63 H, 5.96; N, 10.14.

4.8.6. 1-(4-(4-((2-(1*H*-indol-3-yl)ethyl)carbamoyl)phenoxy) butyl)quinolin-1-ium bromide (1h)

Orange solid; yield 53%; mp 78–80 °C. ^{1}H NMR (600 MHz, DMSO-d_6): δ 10.84 (s, 1H), 9.67 (d, J = 5.4 Hz, 1H), 9.30 (d, J = 8.4 Hz, 1H), 8.66 (d, J = 9.0 Hz, 1H), 8.54–8.48 (m, 2H), 8.32–8.16 (m, 2H), 8.12–7.99 (m, 1H), 7.87–7.78 (m, 2H), 7.57 (d, J = 7.8 Hz, 1H), 7.33 (d, J = 8.4 Hz, 1H), 7.17 (s, 1H), 7.05 (t, J = 7.8 Hz, 1H), 7.01–6.89 (m, 3H), 5.18 (t, J = 7.8 Hz, 2H), 4.08 (t, J = 6.6 Hz, 2H), 3.56–3.50 (m, 2H), 2.94 (t, J = 7.2 Hz, 2H), 2.18–2.09 (m, 2H), 1.93–1.86 (m, 2H). ^{13}C NMR (150 MHz, DMSO-d_6): δ 165.56, 160.58, 147.43, 137.40, 136.20, 135.62, 130.76, 129.85, 129.73, 128.95, 127.26, 126.89, 122.53, 122.16, 120.87, 118.92, 118.30, 118.17, 113.88, 111.94, 111.36., 67.00, 56.94, 40.11, 26.34, 25.45, 25.28. MS (EI) m/z: 464.1 $(M\text{-}Br)^+$. Anal. Calcd For $C_{30}H_{30}BrN_3O_2$: C, 66.18; H, 5.55; N, 7.72. Found: C, 66.21; H, 5.30; N, 7.70.

4.8.7. 1-(4-(4-((2-acetylphenyl)carbamoyl)phenoxy) butyl)quinolin-1-ium bromide (2a)

White solid; yield 79%; mp 167–169 °C. ^{1}H NMR (600 MHz, DMSO-d_6): δ 12.35 (s, 1H),9.62(d, J = 8.4 Hz, 1H) , 9.32 (d, J = 8.4 Hz, 1H), 8.70–8.59 (m,2H), 8.50 (t, J = 8.4 Hz, 1H), 8.36–8.18 (m, 2H), 8.16–8.05 (m, 2H), 7.96–7.90 (m, 2H), 7.68 (t, J = 7.8 Hz, 1H), 7.26 (t, J = 7.8 Hz, 1H), 7.15–7.10 (m, 2H), 5.17 (t, J = 7.2 Hz, 2H), 4.16 (t, J = 7.2 Hz, 2H), 2.71 (s, 3H), 2.27–2.14 (m, 2H), 1.97–1.81 (m, 2H). ^{13}C NMR (100 MHz, DMSO-d_6): δ 203.52, 164.37, 161.45, 140.27, 137.33, 136.89, 135.58, 134.66, 132.24, 129.67, 128.95, 127.17, 126.28, 125.82, 122.75, 122.13, 119.91, 118.95,114.61,67.20, 56.83, 28.75, 26.30, 25.37. MS (EI) m/z: 439.8 $(M\text{-}Br)^+$. Anal. Calcd For $C_{28}H_{27}BrN_2O_3$: C, 64.74; H, 5.24; N, 5.39. Found: C, 64.85; H, 5.35; N, 5.17.

4.8.8. 2-(4-(4-((2-acetylphenyl)carbamoyl)phenoxy) butyl)isoquinolin-2-ium bromide (2b)

White solid; yield 81%; mp 181–183 °C; ^{1}H NMR (400 MHz, DMSO-d_6): δ 12.30 (s, 1H), 10.32 (s, 1H), 8.94 (d, J = 6.6 Hz, 1H), 8.64 (d, J = 6.6 Hz, 2H), 8.51 (d, J = 8.4 Hz, 1H), 8.36 (d, J = 8.4 Hz, 1H), 8.24 (t, J = 7.8 Hz, 1H), 8.07 (t, J = 9.6 Hz, 2H), 7.88 (d, J = 8.4 Hz, 2H), 7.64 (t, J = 7.8 Hz, 1H), 7.21 (t, J = 7.8 Hz, 1H), 7.10 (d, J = 8.4 Hz, 2H), 4.88 (t, J = 7.2 Hz, 2H), 4.13 (t, J = 6.0 Hz, 2H), 2.32–2.16 (m, 2H), 1.90–1.79 (m, 2H). ^{13}C NMR (100 MHz, DMSO-d_6): δ 203.56, 164.39, 161.47, 150.02, 140.04, 136.91, 136.73, 134.92, 134.69, 132.27, 131.06, 130.31, 128.96, 127.17, 126.33, 125.84, 122.82, 122.71, 119.95, 114.63, 67.18, 60.25, 28.76, 27.38, 25.18. MS (EI) m/z: 439.1 $(M\text{-}Br)^+$. Anal. Calcd for $C_{28}H_{27}BrN_2O_3$: C, 64.74; H, 5.24; N, 5.39. Found: C, 64.73; H, 5.26; N, 5.30.

4.8.9. 2-(5-(4-((2-acetylphenyl)carbamoyl)phenoxy)pentyl) isoquinolin-2-ium bromide (2c)

White solid; yield 81%; mp 141–143 °C; ^{1}H NMR (600 MHz, DMSO-d_6): δ 12.33 (s, 1H), 10.14 (s, 1H), 8.84 (d, J = 6.6 Hz, 1H), 8.67 (d, J = 8.4 Hz, 1H), 8.62 (d, J = 6.6 Hz, 1H), 8.49 (d, J = 8.4 Hz, 1H), 8.36 (d, J = 7.8 Hz, 1H), 8.27 (t, J = 7.8 Hz, 1H), 8.12 (d, J = 8.4 Hz, 1H), 8.08 (t, J = 7.8 Hz, 1H), 7.92 (d, J = 8.4 Hz, 2H), 7.68 (t, J = 7.8 Hz, 1H), 7.25 (t, J = 7.8 Hz, 1H), 7.10 (d, J = 8.4 Hz, 2H), 4.77 (t, J = 7.2 Hz, 2H), 4.10 (t, J = 6.0 Hz, 2H), 2.70 (s, 3H), 2.18–2.08 (m, 2H), 1.88–1.79 (m, 2H), 1.56–1.48 (m, 2H). ^{13}C NMR (100 MHz, DMSO-d_6): δ 203.58, 164.43, 161.63, 149.93, 140.06, 136.88, 136.74, 134.93, 134.70, 132.28, 131.09, 130.29, 128.98, 127.22, 127.15, 126.22, 125.81, 122.81, 119.94, 114.58, 67.45, 60.45, 30.14, 28.77, 27.89, 22.06. MS (EI) m/z: 453.3 $(M\text{-}Br)^+$. Anal. Calcd for $C_{29}H_{29}BrN_2O_3$: C, 65.29; H, 5.48; N, 5.25. Found: C, 65.28; H, 5.38; N, 4.96.

4.8.10. 2-(6-(4-((2-acetylphenyl)carbamoyl)phenoxy)hexyl) isoquinolin-2-ium bromide (2d)

White solid; yield 85%, mp 145–147 °C; ^{1}H NMR (600 MHz, DMSO-d_6): δ 12.35 (s, 1H), 10.16 (s, 1H), 8.85 (d, J = 7.2 Hz, 1H), 8.68 (d, J = 7.8 Hz, 1H), 8.62 (d, J = 6.6 Hz, 1H), 8.50 (d, J = 8.4 Hz, 1H), 8.36 (d, J = 8.4 Hz, 1H), 8.27 (t, J = 7.8 Hz, 1H), 8.13 (d, J = 7.8 Hz, 1H), 8.09 (t, J = 7.8 Hz, 1H), 7.92 (d, J = 8.4 Hz, 2H), 7.68 (t, J = 7.8 Hz, 1H), 7.26 (t, J = 7.8 Hz, 1H), 7.10 (d, J = 8.4 Hz, 2H), 4.75 (t, J = 7.2 Hz, 2H), 4.07 (t, J = 6.6 Hz, 2H), 2.71 (s, 3H), 2.11–2.02 (m, 2H), 1.80–1.73 (m, 2H), 1.54–1.47 (m, 2H), 1.45–1.39 (m, 2H). ^{13}C NMR (100 MHz, DMSO-d_6): δ 203.55, 164.45, 161.68, 150.01, 140.05, 136.87, 136.71, 134.95, 134.66, 132.24, 131.05, 130.32, 129.01, 127.23, 127.18, 126.18, 125.81, 122.92, 122.72,

120.02, 114.55, 67.65, 60.52, 30.41, 28.75, 28.20, 25.18, 24.93. MS (EI) *m*/*z*: 467.0 (M-Br)$^+$. Anal. Calcd For $C_{30}H_{31}BrN_2O_3$: C, 65.81; H, 5.71; N, 5.12. Found: C, 65.74; H, 5.99; N, 5.32.

4.8.11. 1-(5-(4-((2-acetylphenyl)carbamoyl)phenoxy) pentyl)quinolin-1-ium bromide (2e)

White solid; yield 81%; mp 133–135 °C; ^{1}H NMR (600 MHz, DMSO-d_6): δ 12.34 (s, 1H), 9.62 (d, J = 4.8 Hz, 1H), 9.32 (d, J = 8.4 Hz, 1H), 8.67 (d, J = 8.4 Hz, 2H), 8.51 (d, J = 8.4 Hz, 1H), 8.33–8.25 (m, 1H), 8.21 (t, J = 6.6 Hz, 1H), 8.12 (d, J = 9.6 Hz, 1H), 8.07 (t, J = 7.8 Hz, 1H), 7.93 (d, J = 8.4 Hz, 2H), 7.68 (t, J = 7.2 Hz, 1H), 7.25 (t, J = 7.2 Hz, 1H), 7.10 (d, J = 8.4 Hz, 2H), 5.13 (t, J = 7.2 Hz, 2H), 4.09 (t, J = 5.4 Hz, 2H), 2.71 (s, 3H), 2.11–2.04 (m, 2H), 1.86–1.79 (m, 2H), 1.62–1.55 (m, 2H). ^{13}C NMR (100 MHz, DMSO-d_6): δ 203.63, 164.47, 161.6, 149.64, 147.40, 140.08, 137.36, 135.65, 134.73, 132.31, 130.74, 129.84, 129.70, 129.02, 126.26, 122.85, 122.75, 122.14, 119.98, 118.99, 114.61, 67.55, 57.15, 29.23, 28.78, 27.97, 22.43. MS (EI) *m*/*z*: 453.3 (M-Br)$^+$. Anal. Calcd for $C_{29}H_{29}BrN_2O_3$: C, 65.29; H, 5.48; N, 5.25. Found: C, 65.45; H, 5.72; N, 5.18.

4.8.12. 1-(5-(4-((2-acetylphenyl)carbamoyl)phenoxy) pentyl)pyridin-1-ium bromide (2f)

White solid; yield 85%; mp 180–182 °C; ^{1}H NMR^{1}H NMR (600 MHz, DMSO-d_6): δ 12.35 (s, 1H), 9.13 (d, J = 6.0 Hz, 2H), 8.67 (d, J = 8.4 Hz, 1H), 8.62 (t, J = 7.8 Hz, 1H), 8.18 (t, J = 7.2 Hz, 2H), 8.13 (d, J = 7.2 Hz, 1H), 7.93 (d, J = 8.4 Hz, 2H), 7.68 (t, J = 7.8 Hz, 1H), 7.25 (t, J = 7.2 Hz, 1H), 7.12 (d, J = 8.4 Hz, 2H), 4.66 (t, J = 7.2 Hz, 2H), 4.09 (t, J = 6.0 Hz, 2H), 2.71 (s, 3H), 2.06–1.96 (m, 2H), 1.86–1.76 (m, 2H), 1.50–1.42 (m, 2H). ^{13}C NMR (100 MHz, DMSO-d_6): δ 203.59, 164.46, 161.65, 145.45, 144.77, 140.06, 134.71, 132.28, 129.01, 128.06, 126.27, 122.89, 120.00, 114.62, 67.45, 60.46, 30.39, 28.77, 27.82, 21.97. MS (EI) *m*/*z*: 403.2 (M-Br)$^+$. Anal. Calcd for $C_{25}H_{27}BrN_2O_3$: C, 62.12; H, 5.63; N, 5.80. Found: C, 62.03; H, 5.63; N, 5.58.

4.8.13. 1-(6-(4-((2-acetylphenyl)carbamoyl)phenoxy)hexyl)pyridin-1-ium bromide (2g)

White solid; yield 75%; mp 78–79 °C; ^{1}H NMR (600 MHz, DMSO-d_6): δ 12.35 (s, 1H), 9.15 (d, J = 6.0 Hz, 2H), 8.67 (d, J = 8.4 Hz, 1H), 8.62 (t, J = 7.8 Hz, 1H), 8.18 (t, J = 6.6 Hz, 2H), 8.12 (d, J = 7.8 Hz, 1H), 7.94 (d, J = 8.4 Hz, 2H), 7.68 (t, J = 7.8 Hz, 1H), 7.25 (t, J = 7.8 Hz, 1H), 7.12 (d, J = 8.4 Hz, 2H), 4.64 (t, J = 7.2 Hz, 2H), 4.07 (t, J = 6.6 Hz, 2H), 2.71 (s, 3H), 2.02–1.92 (m, 2H), 1.81–1.70 (m, 2H), 1.52–1.44 (m, 2H), 1.43–1.31 (m, 2H). ^{13}C NMR (100 MHz, DMSO-d_6): δ 203.58, 164.53, 161.73, 145.47, 144.85, 140.04, 134.68, 132.24, 129.08, 128.07, 126.22, 123.08, 122.80, 120.11, 114.61, 67.65, 60.53, 30.72, 28.78, 28.23, 25.11, 24.88. MS (EI) *m*/*z*: 417.9 (M-Br)$^+$. Anal. Calcd for $C_{26}H_{29}BrN_2O_3$: C, 62.78; H, 5.88; N, 5.63. Found: C, 62.77; H, 6.03; N, 5.53.

4.9. AChE and BChE activity assay

Our assays on the in vitro inhibition of AChE and BChE were measured by a modification of methods previously reported in the literature.[47,48] Recombinant human AChE and BChE obtained from Sigma–Aldrich Company were dissolved in 0.1 M potassium phosphate, pH 7.0. Acetylthiocholine (ATC) and 5′,5′-dithio-bis (2-nitrobenzoic acid) (DTNB) purchased from Sigma–Aldrich Company were prepared in water as stock solutions of 0.01 M and frozen at −20 °C. The reaction mixture in a total assay volume of 200 μL contained appropriate amounts of ATC, DTNB, 0.1 M potassium phosphate buffer, inhibitor and enzyme. Enzymatic hydrolysis of ATC was monitored (microplate reader, BioTek) at 415 nm in the presence or absence of various concentrations of inhibitor at 30 °C, in 0.1 M potassium phosphate, pH 7.0. Each experiment was repeated at least three times and the values were averaged. The inhibition constant (K_i), the indication of an inhibitor's potency, was obtained from the Dixon plot of plotting 1/v against concentration of inhibitor at certain concentrations of substrate. Bovine serum albumin is usually added up to 0.5% of the total reaction volume to reduce the coating of target enzyme during the incubation. In our assay, no obvious effect from bovine serum albumin on the activity of the compounds has been found, which indicates that the new compounds selectively inhibited the target enzyme but not interacted with bovine serum albumin.

4.10. Self-mediated Aβ (1–42) aggregation assay

The thioflavin T based fluorometric assay was used here to investigate the self-mediated Aβ (1–42) aggregation.[46,49–51] Aβ (1–42) samples (GL Biochem, Shanghai) were dissolved in DMSO as a stable stock solution (Aβ = 5 mM). Experiments were performed by shaking the peptide in 50 mM phosphate buffer (pH 8.5) containing 100 mM NaCl at 37 °C for 10 h (final Aβ concentration 100 μM) with and without the tested compound at various concentrations. After incubation, 20 μL of the above solutions were diluted to a final volume of 200 μL with 50 mM glycine-NaOH buffer (pH 8.5) containing 10 μM thioflavin T. Then the measurement of fluorescence intensity was carried out (λ_{exc} = 450 nm, λ_{em} = 480 nm) by microplate reader (SpectraMax M5, Molecular Devices) using black microwell plates (96 wells), and values at the plateau were calculated after subtraction of the background fluorescence of the 10 μM thioflavin T solution.

4.11. β-Secretase inhibition assay

β-Secretase in vitro assay was performed as described in the following procedure by employing the β-secretase fluorescence resonance energy transfer assay kit (P2985, PanVera) according to the literature reports.[39,42] The weakly fluorescent substrate becomes highly fluorescent once the enzymatic cleavage occurs and the increase in fluorescence is linearly correlated with the rate of proteolysis. The detailed procedures are as follows: various concentrations of test compound (5 μL) or DMSO (control), and appropriate amounts of enzyme (20 μL) were preincubated in 50 mM sodium acetate (pH 4.5) at 25 °C. The substrate (150 nM Rhodamine-EVNLDAEFK-quencher) was then added to start the reaction and incubated for 60 min at the same temperature. The fluorescence signal was recorded at λ_{em} = 585 nm (λ_{exc} = 535 nm) by microplate reader (Infinite F200 PRO, Tecan) using black microwell (96 wells). The inhibition percentages corresponding to the presence of different concentrations of test compound was calculated by the following equation: $100 - [(F_i/F_o) \times 100]$, where F_i nd F_o are the fluorescence intensities obtained for β-secretase in the presence and absence of an inhibitor, respectively. The inhibition curve was obtained by plotting the inhibition percentage versus the logarithm of the inhibitor concentration in the reaction system. The linear regression parameters were determined and the IC_{50} was extrapolated with Origin ver. 8.0 software.

4.12. Molecular docking and solvated interaction energies (SIE) calculation

Based on the crystal structure, the AutoDock 4.0 program was applied to dock these inhibitors into the active site of human AChE, and the Gasteiger charges were used for these inhibitors. To select the best set of docking parameters and test the reliability of the docking results, the title compounds were docked into the active site. In the docking process, the Lamarckian genetic algorithm (LGA)[52] was used for the conformational search. Among a series

of docking parameters, the grid size was set to be $30 \times 50 \times 40$, and used grid space was the default value of 0.375 Å. The interaction energy that resulted from probing the AChE with the title compound was assessed by the standard AutoDock scoring function. Among the set of 50 candidates of the docked complex structure, the best one was selected according to the interaction energy and the binding conformation. The same set of the docking parameters were adopted in the molecular docking of other inhibitors. All the complex structures derived from molecular docking were used as starting structures for further energy minimizations using the Sander module of the Amber 8 program before the final structures were achieved. The atomic charges used for these inhibitors were the restrained electrostatic potential (RESP) charges, determined by using the standard RESP procedure implemented in the Antechamber module of the Amber 8 program following the electronic structure and electrostatic potential calculations at the HF/6-31G* level. The energy minimization process was similar to that used for modeling other systems previously, that is, first fixing the backbone atoms of the protein, in order to relax the side chains and the docked inhibitor molecule. Energy minimization was then performed on the whole complex until the convergence criterion of 0.001 kcal mol^{-1} $Å^{-1}$ was reached.

The binding free energy calculations were performed by the SIE method. Similar to MMPBSA/GBSA, SIE treats the protein–ligand system in atomistic detail and solvation effects implicitly. The free energy of binding between ligand and protein is computed by:

$$\Delta G_{bind}(\rho, D_{in}, \alpha, \gamma, C) = \alpha[\Delta E_{VDW} + \Delta E_{Coul}(D_{in}) + \Delta G_{RF}(\rho, D_{in}) + \gamma \Delta SA(\rho)] + C \quad (1)$$

where ΔE_{VDW} and ΔE_{Coul} are the intermolecular van der Waals and Coulomb interaction energies between protein and ligand, ΔG_{RF} (ρ, D_{in}) is the difference in the reaction-field energy between the bound and free state of the protein–ligand complex as calculated by solving the Poisson equation with BRI BEM,[53,54] and $\Delta SA(\rho)$ is the difference in molecular surface area between the bound and free state of the protein. The five parameters in the above equation were fitted to the absolute free energy of binding of 99 protein–ligand complexes: The linear scaling factor ρ of the van der Waals radii of the AMBER99 force field, the dielectric constant inside the solute D_{in}, the coefficient γ for quantifying the free energy associated with the difference in surface area upon protein–ligand binding, and the prefactor α that implicitly quantifies the loss of entropy upon binding, also known as entropy-enthalpy compensation, and a constant C that includes protein-dependent contributions not explicitly modeled by the SIE methodology, for example, the change in protein internal energy upon ligand binding. The default values of the parameters are: $\rho = 1.1$, $D_{in} = 2.25$, $\gamma = 0.0129$ kcal/(mol $Å^2$), $C = -2.89$ kcal/mol, and $\alpha = 0.1048$.

Acknowledgments

The research was supported in part by the National Basic Research Program of China (No. 2010CB126103), the NSFC (No. 20902034, 20925206 and 21102052) and the National Key Technologies RD Program (2011BAE06B05).

References and notes

1. Schmidt, C.; Wolff, M.; Weitz, M.; Bartlau, T.; Korth, C.; Zerr, I. *Arch. Neurol.* **2011**, *68*, 1124.
2. Tomiyama, T.; Shoji, A.; Kataoka, K.; Suwa, Y.; Asano, S.; Kaneko, H.; Endo, N. *J. Biol. Chem.* **1996**, *271*, 6839.
3. Krall, W. J.; Sramek, J. J.; Cutler, N. R. *Ann. Pharmacother.* **1999**, *33*, 441.
4. Lahiri, D. K.; Farlow, M. R.; Sambamurti, K.; Greig, N. H.; Giacobini, E.; Schneider, L. S. *Curr. Drug Targets* **2003**, *4*, 97.
5. Cummings, J. L. *Rev. Neurol. Dis.* **2004**, *1*, 60.
6. Andrisano, V.; Bartolini, M.; Bertucci, C.; Bolognesi, M. L.; Cavalli, A.; Melchiorre, C. *ChemBioChem* **2007**, *8*, 2152.
7. Gauthier, S.; Poirier, J. *Alzheimer Dement* **2008**, *4*, 48.
8. Wolfe, M. S. *Nat. Rev. Drug Discovery* **2002**, *1*, 859.
9. Di Carlo, M.; Giacomazza, D.; San Biagio, P. L. *J. Phys.: Condens. Matter* **2012**, *24*, 244102.
10. Contestabile, A. *Behav. Brain Res.* **2011**, *221*, 334.
11. Giacobini, E. *Pharmacol. Res.* **2004**, *50*, 433.
12. Terry, A. V., Jr.; Buccafusco, J. J. *J. Pharmacol. Exp. Ther.* **2003**, *306*, 821.
13. Savini, L.; Gaeta, A.; Fattorusso, C.; Catalanotti, B.; Campiani, G.; Chiasserini, L.; Pellerano, C.; Novellino, E.; McKissic, D.; Saxena, A. *J. Med. Chem.* **2003**, *46*, 1.
14. Bihel, F.; Das, C.; Bowman, M. J.; Wolfe, M. S. *J. Med. Chem.* **2004**, *47*, 3931.
15. Carlier, P. R.; Du, D. M.; Han, Y.; Liu, J.; Pang, Y. P. *Bioorg. Med. Chem. Lett.* **1999**, *9*, 2335.
16. Pang, Y. P.; Quiram, P.; Jelacic, T.; Hong, F.; Brimijoin, S. *J. Biol. Chem.* **1996**, *271*, 23646.
17. Camps, P.; Munoz-Torrero, D. *Mini-Rev. Med. Chem.* **2001**, *1*, 163.
18. Camps, P.; Formosa, X.; Galdeano, C.; Gomez, T.; Munoz-Torrero, D.; Scarpellini, M.; Viayna, E.; Badia, A.; Clos, M. V.; Camins, A.; Pallas, M.; Bartolini, M.; Mancini, F.; Andrisano, V.; Estelrich, J.; Lizondo, M.; Bidon-Chanal, A.; Luque, F. J. *J. Med. Chem.* **2008**, *51*, 3588.
19. Alonso, D.; Dorronsoro, I.; Rubio, L.; Munoz, P.; Garcia-Palomero, E.; Del Monte, M.; Bidon-Chanal, A.; Orozco, M.; Luque, F. J.; Castro, A.; Medina, M.; Martinez, A. *Bioorg. Med. Chem.* **2005**, *13*, 6588.
20. Luo, W.; Li, Y. P.; He, Y.; Huang, S. L.; Li, D.; Gu, L. Q.; Huang, Z. S. *Eur. J. Med. Chem.* **2011**, *46*, 2609.
21. Munoz-Ruiz, P.; Rubio, L.; Garcia-Palomero, E.; Dorronsoro, I.; del Monte-Millan, M.; Valenzuela, R.; Usan, P.; de Austria, C.; Bartolini, M.; Andrisano, V.; Bidon-Chanal, A.; Orozco, M.; Luque, F. J.; Medina, M.; Martinez, A. *J. Med. Chem.* **2005**, *48*, 7223.
22. Wiesner, J.; Kriz, Z.; Kuca, K.; Jun, D.; Koca, J. *J. Enzyme Inhib. Med. Chem.* **2007**, *22*, 417.
23. Bourne, Y.; Grassi, J.; Bougis, P. E.; Marchot, P. *J. Biol. Chem.* **1999**, *274*, 30370.
24. Kryger, G.; Harel, M.; Giles, K.; Toker, L.; Velan, B.; Lazar, A.; Kronman, C.; Barak, D.; Ariel, N.; Shafferman, A.; Silman, I.; Sussman, J. L. *Acta Crystallogr. D Biol. Crystallogr.* **2000**, *56*, 1385.
25. Cavalli, A.; Bolognesi, M. L.; Minarini, A.; Rosini, M.; Tumiatti, V.; Recanatini, M.; Melchiorre, C. *J. Med. Chem.* **2008**, *51*, 347.
26. Camps, P.; El Achab, R.; Morral, J.; Munoz-Torrero, D.; Badia, A.; Banos, J. E.; Vivas, N. M.; Barril, X.; Orozco, M.; Luque, F. J. *J. Med. Chem.* **2000**, *43*, 4657.
27. Wim, D.; Alfred, H. *J. Org. Chem.* **1991**, *56*, 896.
28. Miao, Y. P.; Wen, R.; Aoshima, H.; Zhou, P. G. *Acta Pharmacol. Sin.* **2004**, *39*, 37.
29. Bo, Z. S.; Zhang, W. K.; Zhang, X.; Zhang, C. M.; Shen, J. C. *Macromol. Chem. Phys.* **1998**, *199*, 1323.
30. Harel, M.; Schalk, I.; Ehret-Sabatier, L.; Bouet, F.; Goeldner, M.; Hirth, C.; Axelsen, P. H.; Silman, I.; Sussman, J. L. *Proc. Natl. Acad. Sci. U.S.A.* **1993**, *90*, 9031.
31. Bourne, Y.; Taylor, P.; Radic, Z.; Marchot, P. *EMBO J.* **2003**, *22*, 1.
32. Hao, G. F.; Wang, F.; Li, H.; Zhu, X. L.; Yang, W. C.; Huang, L. S.; Wu, J. W.; Berry, E. A.; Yang, G. F. *J. Am. Chem. Soc.* **2012**. http://dx.doi.org/10.1021/ja3001908.
33. Zhao, P. L.; Wang, L.; Zhu, X. L.; Huang, X.; Zhan, C. G.; Wu, J. W.; Yang, G. F. *J. Am. Chem. Soc.* **2010**, *132*, 185.
34. Huff, F. J.; Reiter, C. T.; Rand, J. B. *J. Neural Transm. Suppl.* **1989**, *75*, 129.
35. Dvir, H.; Silman, I.; Harel, M.; Rosenberry, T. L.; Sussman, J. L. *Chem. Biol. Interact.* **2010**, *187*, 10.
36. Minarini, A.; Milelli, A.; Tumiatti, V.; Rosini, M.; Simoni, E.; Bolognesi, M. L.; Andrisano, V.; Bartolini, M.; Motori, E.; Angeloni, C.; Hrelia, S. *Neuropharmacology* **2012**, *62*, 997.
37. Jiang, H.; Wang, X.; Huang, L.; Luo, Z.; Su, T.; Ding, K.; Li, X. *Bioorg. Med. Chem.* **2011**, *19*, 7228.
38. Camps, P.; Formosa, X.; Galdeano, C.; Munoz-Torrero, D.; Ramirez, L.; Gomez, E.; Isambert, N.; Lavilla, R.; Badia, A.; Clos, M. V.; Bartolini, M.; Mancini, F.; Andrisano, V.; Arce, M. P.; Rodriguez-Franco, M. I.; Huertas, O.; Dafni, T.; Luque, F. J. *J. Med. Chem.* **2009**, *52*, 5365.
39. Piazzi, L.; Cavalli, A.; Colizzi, F.; Belluti, F.; Bartolini, M.; Mancini, F.; Recanatini, M.; Andrisano, V.; Rampa, A. *Bioorg. Med. Chem. Lett.* **2008**, *18*, 423.
40. Bolognesi, M. L.; Minarini, A.; Rosini, M.; Tumiatti, V.; Melchiorre, C. *Mini-Rev. Med. Chem.* **2008**, *8*, 960.
41. Cavalli, A.; Bolognesi, M. L.; Capsoni, S.; Andrisano, V.; Bartolini, M.; Margotti, E.; Cattaneo, A.; Recanatini, M.; Melchiorre, C. *Angew. Chem., Int. Ed.* **2007**, *46*, 3689.
42. Al-Tel, T. H.; Semreen, M. H.; Al-Qawasmeh, R. A.; Schmidt, M. F.; El-Awadi, R.; Ardah, M.; Zaarour, R.; Rao, S. N.; El-Agnaf, O. *J. Med. Chem.* **2011**, *54*, 8373.
43. Sankaranarayanan, S.; Price, E. A.; Wu, G.; Crouthamel, M. C.; Shi, X. P.; Tugusheva, K.; Tyler, K. X.; Kahana, J.; Ellis, J.; Jin, L.; Steele, T.; Stachel, S.; Coburn, C.; Simon, A. J. *J. Pharmacol. Exp. Ther.* **2008**, *324*, 957.
44. Durham, T. B.; Shepherd, T. A. *Curr. Opin. Drug Discov. Devel.* **2006**, *9*, 776.
45. Citron, M. *Trends Pharmacol. Sci.* **2004**, *25*, 92.
46. Bartolini, M.; Bertucci, C.; Bolognesi, M. L.; Cavalli, A.; Melchiorre, C.; Andrisano, V. *ChemBioChem* **2007**, *8*, 2152.
47. Yang, W.; Xue, L.; Fang, L.; Chen, X.; Zhan, C. G. *Chem. Biol. Interact.* **2010**, *187*, 148.
48. Ellman, G. L.; Courtney, K. D.; Andres, V., Jr.; Feather-Stone, R. M. *Biochem. Pharmacol.* **1961**, *7*, 88.
49. LeVine, H., 3rd *Protein Sci.* **1993**, *2*, 404.
50. Naiki, H.; Higuchi, K.; Nakakuki, K.; Takeda, T. *Lab. Invest.* **1991**, *65*, 104.

51. Bolognesi, M. L.; Banzi, R.; Bartolini, M.; Cavalli, A.; Tarozzi, A.; Andrisano, V.; Minarini, A.; Rosini, M.; Tumiatti, V.; Bergamini, C.; Fato, R.; Lenaz, G.; Hrelia, P.; Cattaneo, A.; Recanatini, M.; Melchiorre, C. *J. Med. Chem.* **2007**, *50*, 4882.
52. Morris, G. M.; Goodsel, D. S.; Halliday, R. S.; Huey, R.; Hart, W. E.; Belew, R. K.; Olson, A. J. *J. Comput. Chem.* **1998**, *19*, 1639.
53. Purisima, E. O. *J. Comput. Chem.* **1998**, *19*, 1494.
54. Purisima, E. O.; Nilar, S. H. *J. Comput. Chem.* **1995**, *16*, 681.